PAPER

Check for updates

Near-infrared-IIb probe affords ultrahigh contrast inflammation imaging†

Cong Hua, *[a] Biao Huang, [b] Yingying Jiang, [c] Shoujun Zhu[cd] and Ran Cui [ID] *[b]

Deep tissue imaging in the near-infrared II (NIR-II) window with significantly reduced tissue autofluorescence and scattering provides an important modality to visualize various biological events. Current commercially used contrast agents in the near-infrared spectrum suffer from severe photobleaching, high tissue scattering, and background signals, hampering high-quality *in vivo* bioimaging, particularly in small animals. Here, we applied a NIR-IIb quantum dot (QD) probe with greatly suppressed photon scattering and zero autofluorescence to map inflammatory processes. Two-layer surface modification by a combination of amphiphilic polymer and mixed linear and multi-armed polyethylene glycol chains prolonged probe circulation *in vivo* and improved its accumulation in the inflammation sites. Compared to indocyanine green, a widely applied dye in the clinic, our QD probe showed greater photostability and capacity for deeper tissue imaging with superior contrast. The longer circulation of QDs also improved vessel imaging, which is vital for better understanding of biological mechanisms of the inflammation microenvironment. Our proposed NIR-IIb *in vivo* imaging modality proved effective for the visualization of inflammation in small animals, and its use may be extended in future to studies of immunity and cancer.

Introduction

Inflammation is a very important physiological process that represents an adaptive response to noxious events following infection and tissue injury.[1] Although the types of inflammatory processes and their interrelations have been described in detail, the physiological mechanisms of inflammation, particularly during chronic infections, are not completely understood. Such mechanisms are especially complicated for systemic chronic inflammation, which is associated with diseases such as metabolic disorder and cardiovascular diseases.[1–7] Inflammation in response to infection is mediated by the components of the innate immune system, such as local macrophages and mast cells.[8] Mapping in detail the processes and microenvironment of inflammation by an *in vivo* imaging modality[9,10] enables to characterize the key events in the induction of inflammatory response, activation of inflammatory pathways, parainflammation processes and other related phenomena.

Modern biomedical techniques employ a variety of imaging modalities to visualize biological events and disease states.[11–13] Compared to magnetic resonance imaging, computed tomography, positron emission tomography, or single-photon emission computed tomography, optical imaging, especially fluorescence-based imaging, has several advantages with regard to the real-time imaging mode, multicolor labeling, and high resolution.[14,15] Fluorescence imaging has been used with several advanced techniques, such as small animal imaging platform, confocal laser scanning microscopy, and light sheet microscopy, to investigate various biological processes. Fluorescence imaging navigation system has been also applied in the clinical setting, *e.g.*, indocyanine green is successfully used for near-infrared imaging-guided surgery.[16,17] Given that imaging penetration depth is greatly limited by tissue autofluorescence and light scattering, current fluorescence imaging probes for small laboratory animals mainly focus on the red to near-infrared I (NIR-I) range (~600–1000 nm).[18] Imaging at longer wavelengths, particularly in the NIR-II window, enhances visualization of inflammation *in vivo*, affording greater tissue penetration and imaging contrast.[19,20]

In several recent studies, donor–acceptor–donor dyes with NIR-II peak emission[21–30] and cyanine dyes with both NIR-II peak[31,32] and tail emission[33–39] have been successfully applied for NIR-II imaging. However, increasing amount of evidence suggests that the true advantage of NIR-II imaging is achieved in the NIR-IIb sub-window (>1500 nm),[40–43] in which the emission light penetrates different types of tissues with little energy

[a]*Department of Surgical Neuro-oncology, The First Hospital of Jilin University, Changchun, 130061, PR China. E-mail: huacong@jlu.edu.cn*

[b]*College of Chemistry and Molecular Sciences, Wuhan University, Wuhan 430070, PR China. E-mail: cuiran@whu.edu.cn*

[c]*State Key Laboratory of Supramolecular Structure and Materials, College of Chemistry, Jilin University, Changchun 130012, China*

[d]*Key Laboratory of Organ Regeneration & Transplantation of the Ministry of Education, The First Hospital of Jilin University, Changchun, 130061, PR China*

† Electronic supplementary information (ESI) available: Materials, synthesis of quantum dots, NIR-II imaging. See DOI: 10.1039/d0ra06249a

loss and scattering, and with nearly zero autofluorescence. Due to water absorbance at ~1400 nm, the NIR-IIb window can also avoid this usually unavoidable disturbance although it has been claimed that imaging at the peak absorbance of water (near 1450 nm) may provide the highest image contrast in the shortwave infrared.[44] Thus, NIR-IIb imaging has been used to achieve high resolution of mouse vasculature, tumors, lymph nodes and visualize immune therapy process.[41,42,45–48] More importantly, broadening the NIR window from 700 to over 1500 nm may potentially integrate multiple channels for imaging complex biological events.

Based on above background, in the present study we applied a NIR-IIb probe with for ultrahigh contrast imaging of inflammation, enabling future expansion for studies of inflammation microenvironment. The NIR-IIb quantum dot (QD) probe with the core–shell structure was synthesized by using a protocol similar to that described in our previous work.[45–47] The amphiphilic polymer oleylamine-poly(acrylic acid) (OPA) was used to deliver the oil-soluble QDs to a water-soluble phase and a combination of m-polyethyleneglycol (PEG)-amine and 8-arm PEG-amine was used to improve the biocompatibility and in vivo circulation time of the QD probe. The as-prepared QDs enabled high-quality vessel imaging, whereas the prolonged circulation also improved probe accumulation in the sites of inflammation. We demonstrated that our NIR-IIb QD probe provided high imaging quality in a small laboratory animal (inflammation imaging in this work). We also outlined the key challenges that will shape the future application of the probe, particularly with regard to clarifying the origin and physiological roles of the inflammation.

Results and discussion

NIR-IIb probes with extremely low tissue scattering and autofluorescence have afforded ultrahigh imaging contrast and penetration depth.[45–47,49] We initially tested the optimal surface modification and identified a two-layer-surface coating that improved biosafety of QDs (the dynamic light scattering (DLS) size of QDs is about 35 nm and the zeta potential of the QDs is about −1.4 eV). The coated QDs possessed superbright NIR-IIb emission with peak emission at 1600 nm.[45–47] The QDs also exhibited outstanding photostability during the exposure to a high-power 808 nm laser, eliminating quantification problems that could be caused by signal decay. The large Stokes shift, widely recognized to be critical for background signal reduction, improved imaging quality (Fig. 1a). We used a 1% intralipid solution to simulate the tissue to test the penetration depth of the QDs with that of indocyanine green (ICG), a probe used in the clinic.[50] QDs imaging signals were collected in the >1500 nm region. From the fluorescence images of capillaries filled with QDs or ICG solutions, we observed that the former penetrated deeper and significantly improved contrast in the NIR-IIb window (Fig. 1b). Multilayer surface modification with both OPA and PEGylation layers can significantly improve in vivo stability and in vivo circulation time of QDs. We further optimized the surface coating of PbS/CdS core–shell QDs and proved that the two-layer surface coating by OPA and
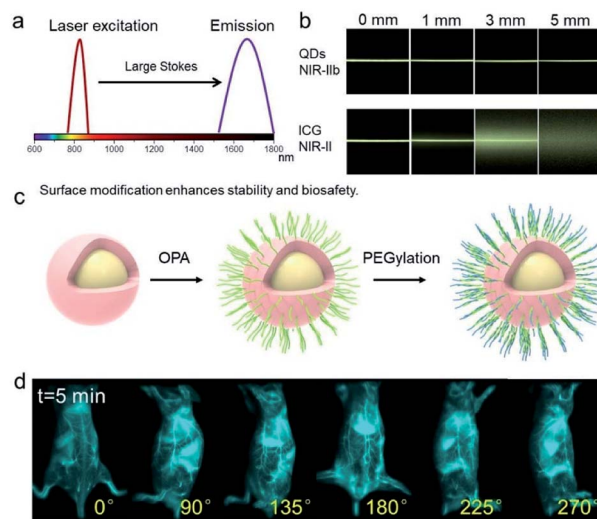

Fig. 1 Imaging with a NIR-IIb probe with extremely low tissue scattering and autofluorescence affords ultrahigh imaging contrast and penetration depth. (a) Scheme of "the large Stokes shift accounts for low background signal and superior imaging quality". (b) Fluorescence images of capillaries filled with aqueous solutions of quantum dots (QDs) and indocyanine green (ICG), covered by a 1% intralipid solution at varying depths. QDs imaging signals were collected in the >1500 nm region. Data was plotted from previous report.[47] (c) Scheme of the PbS/CdS core−shell QDs after coating by OPA and PEGylation. The two-layer surface coating significantly improved the stability and biosafety of QDs. (d) Whole-body rotating images after administration of the NIR-IIb probe into the tail-vein (100−150 µL of 3 µM solution of coated QDs).[47]

PEGylation dramatically improved the stability and biosafety of QDs (Fig. 1c). As shown in Fig. S1,† OPA-coated QDs had short vessel circulation time, whereas further PEGylation greatly enhanced the circulation time and in vivo stability of the NIR-IIb QD probe. The rotated whole body imaging of mice after tail vein administration of the NIR-IIb probe provided high-quality 360° omnidirectional visualization of mouse vessels (Fig. 1d, S2, S3 and Video S1–S3†). The extremely low background signal enabled super-high imaging contrast.

With a well-established NIR-IIb probe in hand, we first tested whether it was suitable for high-quality and high-contrast vessel imaging. To this end, a shaved mouse was immobilized in the supine position with the left leg exposed under the imaging field of view for video-rate hind limb vessel imaging (Fig. 2a and Video S4†). Following an injection of 100–150 µL of 3 µM two-layer coated QDs, the vessel structure was visualized clearly and with extremely low background signal by video-rate imaging under the 1500 nm long pass filter. The hind limb vein was visualized first, and the NIR-IIb signal spread in both the veins and arteries, highlighting the potential of the probe for real-time monitoring of inflammatory processes. Additionally, we performed high-quality vessel imaging in other parts of the body, including leg, backside, abdomen, tail, and others (Fig. 2b). In all cases, our probe allowed for high-quality vessel imaging under surgical light exposure with maximal vessel signal to background (muscle) ratio. Multiplexed NIR-II
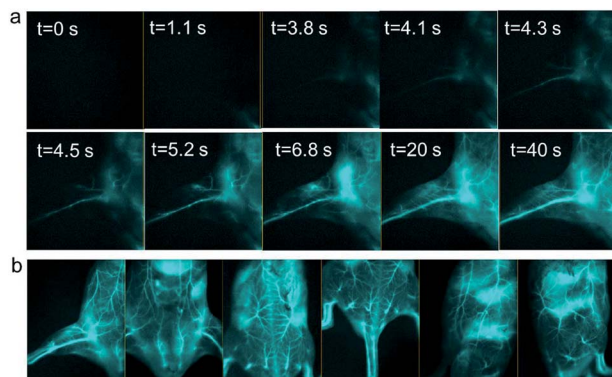
Fig. 2 NIR-IIb probe enables high contrast vessel imaging. (a) The mouse was fixed on the operation platform with the left leg exposed under the imaging field of view. Video-rate images were recorded under 1500 nm long pass filter after tail vein injection of coated NIR-IIb probe. (b) High-quality vessel images visualized at various body parts: leg, abdomen, backside, tail, and lateral side. NIR-II imaging was conducted at the excitation power density of 150 mW cm^{-2} and 808 nm wavelength.[35,47,51,58–60] Due to the energy loss after passing through the 850/1000 nm SP excitation-filter set, the actual exposure power received by the mice was weaker. All 2.5× high-magnification data were simultaneously collected using the same cohort of mice when conducting 1× whole-body imaging during the previous and current projects.[47]

visualization of metastatic tumors and sentinel lymph node resection with full light exposure surgery has been achieved previously.[47] The current study also proves that NIR-IIb imaging modality enables universal navigation under surgical light exposure for both preclinical and clinical procedures.

We next carried out whole body NIR-IIb imaging and traced signal accumulation locations of the coated QDs probes. Because two-layer coated QDs showed improved *in vivo* pharmacokinetic properties compared to those of previous probes with suboptimal surface modifications, we assumed that our probe would remain in blood circulation for longer and would have lower skin uptake in the whole-body imaging mode. Fig. 3a illustrates NIR-IIb imaging of mice in the supine position after administration of QDs under 1500 nm long pass filter and 808 nm laser excitation. Vessels were clearly observed even at >12 h post-injection. NIR-IIb imaging of mice in the lateral position provided even better vessel visualization with extremely low background signals and allowed to map small vessels (Fig. 3b). Statistical analysis of the long-term and short-term liver, skin, and vessel signals at different post-injection time points (Fig. 3c and d) indicated that coated QDs had very low skin uptake due to the rational surface coating with favorable *in vivo* pharmacokinetics. In contrast, low amount of PEGylation precluded high-quality NIR-IIb imaging, particularly during later post-injection time points, and the skin signal appeared at 4 to 20 h post-injection time points (Fig. S4†). It's very hard to rule out the possibility of the QDs being degraded within the body, which needs further investigation. However, previous study indicated that "∼76% of injected QDs were excreted from the body with feces after 4 weeks",[45] which was roughly consistent with current study.
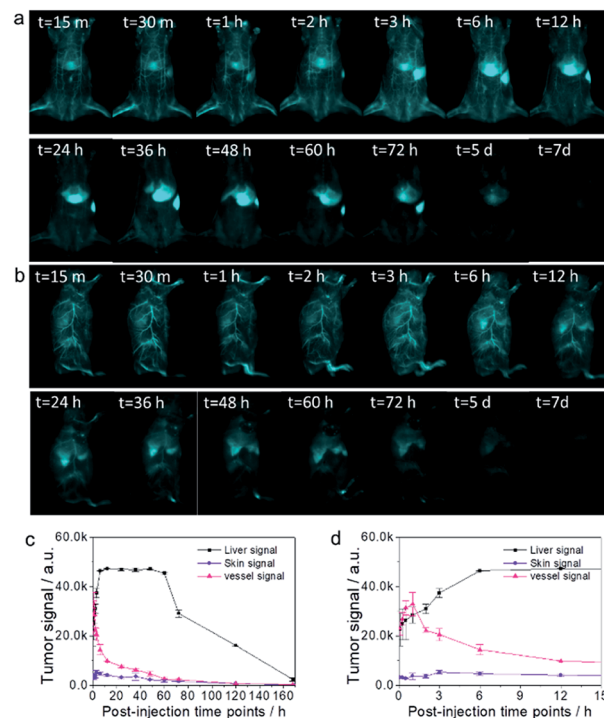

Fig. 3 Circulation and excretion properties of the NIR-IIb probe allow long-term whole body imaging. (a and b) NIR-IIb imaging of a mouse in the supine (a) and lateral (b) positions after administration of the QD probe under 1500 nm long pass filter and 808 nm laser excitation. (c) Magnitude of the liver, skin, vessel signals at different post-injection time points. (d) Rapid absorption dynamics of the QD probe in the liver, skin, and vessels post-injection.

Inflammation is an adaptive response during which chemical and biological substances are released into the blood to protect specific sites of the body, causing increased blood flow in the inflamed areas. The increased number of cells and inflammatory substances within the sites of inflammation augments accumulation of foreign substances.[1] Because large numbers of immune cells accumulate in the sites of inflammation, we hypothesized that they could take up coated QDs probes, enabling targeted high-quality NIR-IIb inflammation imaging. To verify this assumption, a mouse with on-going inflammation was injected with the QD probe through the tail vein (Fig. 4a). NIR-IIb imaging of this mouse at both the supine and lateral positions after the administration of the QD probe under 1500 nm long pass filter and 808 nm laser excitation clearly visualized relatively fast QD probe accumulation with the signal in the inflammation site reaching the peak at around 4–6 h (Fig. 4b and c). Organ distribution of QDs at 24 h post-injection indicated that besides the accumulation in site of inflammation, the QD probe also accumulated in high amounts in the liver, spleen, and lung (Fig. 4e and f).

Next, we examined the accumulation of the QD probe in tumors. SKOV3 tumor cells were inoculated subcutaneously into the armpit of mice, which were monitored until the tumor size reached 0.5 × 0.5 cm. The QD probe was administered to mice with tumors (Fig. S5†) and was found to provide high-
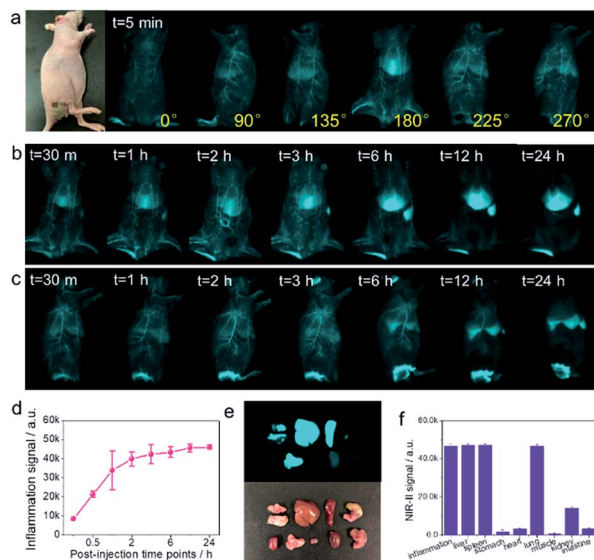
Fig. 4 NIR-IIb probe enables high-quality inflammation imaging. (a) Mouse with an inflammation focus at the base of the tail. (b and c) NIR-IIb imaging of the mouse with inflammation in the supine (b) and lateral (c) positions after administration of the QD probe under 1500 nm long pass filter and 808 nm laser excitation. (d) The magnitude of the signal in the inflammation site after tail vein injection of the QD probe. (e and f) Organ distribution of QDs.

quality NIR-IIb tumor imaging in room light conditions. The 2.5× magnification of the tumor site at early time points after QD probe injection visualized tumor structure in detail (Fig. S5b†). Although a previous study indicated much higher accumulation of the QD probe in the U87 tumor model,[45] it had relatively low accumulation in the SKOV3 tumor model in our present experiments. Whole body NIR-IIb imaging of SKOV3 tumor-bearing mouse (1× magnification) with surrounding inflammation sites at different post-injection time points indicated that the accumulated signal was stronger in the sites of inflammation than in the tumor site. We speculated that inflammation site was looser than the solid-tumor site. In the same conditions of injection dose and imaging set-up, the abundant accumulation of NIR-IIb QDs in the inflammation sites will possibly result in bright NIR-II signal. This point needs further investigation.

Conclusions

Inflammation comprises many physiological and pathological processes.[1] Mechanisms of the acute inflammatory response to the infection are becoming increasingly elucidated. Contemporary experimental and clinical evidence suggests that inflammation has close relationship with many normal and pathological processes, such as metabolism, immunity,[2] metabolic disorders,[3] cancer progression,[6,8] atherosclerosis,[5] autoimmune disease,[4] Alzheimer's disease,[7] and others. However, the exact details of the interrelationships between inflammation and these processes are often not known. Therefore, it is essential to be able to reveal important constituents in the local

microenvironment that mediate inflammatory responses and to develop efficient therapeutic approaches on the basis of this knowledge. The present study describes an important imaging probe for clear visualization of the inflammation process. Application of the proposed NIR-II imaging in combination with confocal[51–53] and light sheet microscopy[42,48] in future will enable detailed studies of the inflammation microenvironment and mechanisms of cancer-related inflammation.

Our NIR-IIb imaging modality provides a potential solution to investigate complex biological events in the real-time manner. A previous study has demonstrated application of dual-channel NIR-II probes for simultaneous metastatic tumor imaging and sentinel lymph node resection with full surgery with light exposure and *in vivo* vessel imaging from both macro- and micromicroscopic dimensions.[45,47] Our probe for imaging at >1500 nm NIR-IIb window with extremely low tissue autofluorescence and scattering affords great penetration depth, high spatial resolution, and real-time imaging speed.[47] NIR-II molecular imaging at longer wavelengths is favorable for muscle, brain, skin and subcutaneous tissues.[54] Our NIR-IIb probe yielded greater spatial resolution and penetration depth by tissues in the NIR-IIb window due to a combination of factors such as low-autofluorescence, minimized photon scattering, water absorption, and large Stokes shift (excitation at 808 nm and signal collection at >1500 nm).[47]

It is widely accepted that imaging at the NIR region has several advantages, particularly for studies *in vivo* and clinical imaging-guided surgery.[14,15,55–57] Current commercial NIR probes mainly focus on the narrow NIR-I window between 700 and 1000 nm. It is very important to extend the imaging emission range for multicolor channels with non-overlapping emission spectra to label different biological processes and objects simultaneously without any crosstalk between channels.[47] This increased wavelength range will provide sufficient space to integrate multiplexed channels and enable real-time visualization of complex biological events with unprecedented imaging contrast and penetration depth in the true NIR-II transparent imaging windows.

Conflicts of interest

There are no conflicts to declare.

Acknowledgements

Notes and references

1 R. Medzhitov, *Nature*, 2008, **454**, 428–435.
2 S. I. Grivennikov, F. R. Greten and M. Karin, *Cell*, 2010, **140**, 883–899.
3 G. S. Hotamisligil, *Nature*, 2006, **444**, 860–867.

4 B. Levine, N. Mizushima and H. W. Virgin, *Nature*, 2011, **469**, 323–335.

5 P. Libby, *Nature*, 2002, **420**, 868–874.

6 A. Mantovani, P. Allavena, A. Sica and F. Balkwill, *Nature*, 2008, **454**, 436–444.

7 H. Akiyama, *Neurobiol. Aging*, 2000, **21**, 383–421.

8 L. M. Coussens and Z. Werb, *Nature*, 2002, **420**, 860–867.

9 M. Zhao, R. Wang, B. Li, Y. Fan, Y. Wu, X. Zhu and F. Zhang, *Angew. Chem., Int. Ed.*, 2019, **58**, 2050–2054.

10 S. Wang, L. Liu, Y. Fan, A. M. El-Toni, M. S. Alhoshan, D. Li and F. Zhang, *Nano Lett.*, 2019, **19**, 2418–2427.

11 Z. Zhou, R. Bai, J. Munasinghe, Z. Shen, L. Nie and X. Chen, *ACS Nano*, 2017, **11**, 5227–5232.

12 X. Sun, X. Huang, J. Guo, W. Zhu, Y. Ding, G. Niu, A. Wang, D. O. Kiesewetter, Z. L. Wang, S. Sun and X. Chen, *J. Am. Chem. Soc.*, 2014, **136**, 1706–1709.

13 Y. Wang, L. Lang, P. Huang, Z. Wang, O. Jacobson, D. O. Kiesewetter, I. U. Ali, G. Teng, G. Niu and X. Chen, *Proc. Natl. Acad. Sci. U. S. A.*, 2015, **112**, 208–213.

14 A. L. Vahrmeijer, M. Hutteman, J. R. van der Vorst, C. J. van de Velde and J. V. Frangioni, *Nat. Rev. Clin. Oncol.*, 2013, **10**, 507–518.

15 R. R. Zhang, A. B. Schroeder, J. J. Grudzinski, E. L. Rosenthal, J. M. Warram, A. N. Pinchuk, K. W. Eliceiri, J. S. Kuo and J. P. Weichert, *Nat. Rev. Clin. Oncol.*, 2017, **14**, 347–364.

16 C. Vinegoni, I. Botnaru, E. Aikawa, M. A. Calfon, Y. Iwamoto, E. J. Folco, V. Ntziachristos, R. Weissleder, P. Libby and F. A. Jaffer, *Sci. Transl. Med.*, 2011, **3**, 84ra45.

17 M. J. Whitley, D. M. Cardona, A. L. Lazarides, I. Spasojevic, J. M. Ferrer, J. Cahill, C. L. Lee, M. Snuderl, D. G. Blazer III, E. S. Hwang, R. A. Greenup, P. J. Mosca, J. K. Mito, K. C. Cuneo, N. A. Larrier, E. K. O'Reilly, R. F. Riedel, W. C. Eward, D. B. Strasfeld, D. Fukumura, R. K. Jain, W. D. Lee, L. G. Griffith, M. G. Bawendi, D. G. Kirsch and B. E. Brigman, *Sci. Transl. Med.*, 2016, **8**, 320ra324.

18 T. Ishizawa, N. Fukushima, J. Shibahara, K. Masuda, S. Tamura, T. Aoki, K. Hasegawa, Y. Beck, M. Fukayama and N. Kokudo, *Cancer*, 2009, **115**, 2491–2504.

19 K. Welsher, Z. Liu, S. P. Sherlock, J. T. Robinson, Z. Chen, D. Daranciang and H. Dai, *Nat. Nanotechnol.*, 2009, **4**, 773–780.

20 G. Hong, S. Diao, J. Chang, A. L. Antaris, C. Chen, B. Zhang, S. Zhao, D. N. Atochin, P. L. Huang, K. I. Andreasson, C. J. Kuo and H. Dai, *Nat. Photonics*, 2014, **8**, 723–730.

21 A. L. Antaris, H. Chen, K. Cheng, Y. Sun, G. Hong, C. Qu, S. Diao, Z. Deng, X. Hu, B. Zhang, X. Zhang, O. K. Yaghi, Z. R. Alamparambil, X. Hong, Z. Cheng and H. Dai, *Nat. Mater.*, 2016, **15**, 235–242.

22 Y. Cai, Z. Wei, C. Song, C. Tang, W. Han and X. Dong, *Chem. Soc. Rev.*, 2019, **48**, 22–37.

23 S. He, J. Song, J. Qu and Z. Cheng, *Chem. Soc. Rev.*, 2018, **47**, 4258–4278.

24 F. Ding, Y. Zhan, X. Lu and Y. Sun, *Chem. Sci.*, 2018, **9**, 4370–4380.

25 S. J. Woo, S. Park, J. E. Jeong, Y. Hong, M. Ku, B. Y. Kim, I. H. Jang, S. C. Heo, T. Wang, K. H. Kim, J. Yang, J. H. Kim and H. Y. Woo, *ACS Appl. Mater. Interfaces*, 2016, **8**, 15937–15947.

26 J. Qi, Y. Fang, R. T. K. Kwok, X. Zhang, X. Hu, J. W. Y. Lam, D. Ding and B. Z. Tang, *ACS Nano*, 2017, **11**, 7177–7188.

27 X. D. Zhang, H. Wang, A. L. Antaris, L. Li, S. Diao, R. Ma, A. Nguyen, G. Hong, Z. Ma, J. Wang, S. Zhu, J. M. Castellano, T. Wyss-Coray, Y. Liang, J. Luo and H. Dai, *Adv. Mater.*, 2016, **28**, 6872–6879.

28 B. Guo, Z. Sheng, K. Kenry, D. Hu, X. Lin, S. Xu, C. Liu, H. Zheng and B. Liu, *Mater. Horiz.*, 2017, **4**, 1151–1156.

29 S. Gao, G. Wei, S. Zhang, B. Zheng, J. Xu, G. Chen, M. Li, S. Song, W. Fu, Z. Xiao and W. Lu, *Nat. Commun.*, 2019, **10**, 2206.

30 X. Lu, P. Yuan, W. Zhang, Q. Wu, X. Wang, M. Zhao, P. Sun, W. Huang and Q. Fan, *Polym. Chem.*, 2018, **9**, 3118–3126.

31 E. D. Cosco, J. R. Caram, O. T. Bruns, D. Franke, R. A. Day, E. P. Farr, M. G. Bawendi and E. M. Sletten, *Angew. Chem.*, 2017, **56**, 13126–13129.

32 B. Li, L. Lu, M. Zhao, Z. Lei and F. Zhang, *Angew. Chem.*, 2018, **57**, 7483–7487.

33 A. L. Antaris, H. Chen, S. Diao, Z. Ma, Z. Zhang, S. Zhu, J. Wang, A. X. Lozano, Q. Fan, L. Chew, M. Zhu, K. Cheng, X. Hong, H. Dai and Z. Cheng, *Nat. Commun.*, 2017, **8**, 15269.

34 J. A. Carr, D. Franke, J. R. Caram, C. F. Perkinson, M. Saif, V. Askoxylakis, M. Datta, D. Fukumura, R. K. Jain, M. G. Bawendi and O. T. Bruns, *Proc. Natl. Acad. Sci. U. S. A.*, 2018, **115**, 4465–4470.

35 S. Zhu, Z. Hu, R. Tian, B. C. Yung, Q. Yang, S. Zhao, D. O. Kiesewetter, G. Niu, H. Sun, A. L. Antaris and X. Chen, *Adv. Mater.*, 2018, **30**, e1802546.

36 S. Zhu, B. C. Yung, S. Chandra, G. Niu, A. L. Antaris and X. Chen, *Theranostics*, 2018, **8**, 4141–4151.

37 Z. Starosolski, R. Bhavane, K. B. Ghaghada, S. A. Vasudevan, A. Kaay and A. Annapragada, *PLoS One*, 2017, **12**, e0187563.

38 Z. Hu, C. Fang, B. Li, Z. Zhang, C. Cao, M. Cai, S. Su, X. Sun, X. Shi, C. Li, T. Zhou, Y. Zhang, C. Chi, P. He, X. Xia, Y. Chen, S. S. Gambhir, Z. Cheng and J. Tian, *Nat. Biomed. Eng.*, 2019, **4**, 259.

39 Z. Feng, X. Yu, M. Jiang, L. Zhu, Y. Zhang, W. Yang, W. Xi, G. Li and J. Qian, *Theranostics*, 2019, **9**, 5706–5719.

40 C. N. Zhu, P. Jiang, Z. L. Zhang, D. L. Zhu, Z. Q. Tian and D. W. Pang, *ACS Appl. Mater. Interfaces*, 2013, **5**, 1186–1189.

41 Y. Fan, P. Wang, Y. Lu, R. Wang, L. Zhou, X. Zheng, X. Li, J. A. Piper and F. Zhang, *Nat. Nanotechnol.*, 2018, **13**, 941–946.

42 Y. Zhong, Z. Ma, F. Wang, X. Wang, Y. Yang, Y. Liu, X. Zhao, J. Li, H. Du, M. Zhang, Q. Cui, S. Zhu, Q. Sun, H. Wan, Y. Tian, Q. Liu, W. Wang, K. C. Garcia and H. Dai, *Nat. Biotechnol.*, 2019, **37**, 1322–1331.

43 O. T. Bruns, T. S. Bischof, D. K. Harris, D. Franke, Y. Shi, L. Riedemann, A. Bartelt, F. B. Jaworski, J. A. Carr, C. J. Rowlands, M. W. B. Wilson, O. Chen, H. Wei, G. W. Hwang, D. M. Montana, I. Coropceanu, O. B. Achorn, J. Kloepper, J. Heeren, P. T. C. So, D. Fukumura, K. F. Jensen, R. K. Jain and M. G. Bawendi, *Nat. Biomed. Eng.*, 2017, **1**, 0056.

44 J. A. Carr, M. Aellen, D. Franke, P. T. C. So, O. T. Bruns and M. G. Bawendi, *Proc. Natl. Acad. Sci. U. S. A.*, 2018, **115**, 201803210.

45 M. Zhang, J. Yue, R. Cui, Z. Ma, H. Wan, F. Wang, S. Zhu, Y. Zhou, Y. Kuang, Y. Zhong, D. W. Pang and H. Dai, *Proc. Natl. Acad. Sci. U. S. A.*, 2018, **115**, 6590–6595.

46 Z. Ma, M. Zhang, J. Yue, C. Alcazar, Y. Zhong, T. C. Doyle, H. Dai and N. F. Huang, *Adv. Funct. Mater.*, 2018, **28**, 1803417.

47 R. Tian, H. Ma, S. Zhu, J. Lau, R. Ma, Y. Liu, L. Lin, S. Chandra, S. Wang, X. Zhu, H. Deng, G. Niu, M. Zhang, A. L. Antaris, K. S. Hettie, B. Yang, Y. Liang and X. Chen, *Adv. Mater.*, 2020, **32**, 1907365.

48 F. Wang, H. Wan, Z. Ma, Y. Zhong, Q. Sun, Y. Tian, L. Qu, H. Du, M. Zhang, L. Li, H. Ma, J. Luo, Y. Liang, W. J. Li, G. Hong, L. Liu and H. Dai, *Nat. Methods*, 2019, **16**, 545–552.

49 Y. Zhong, Z. Ma, S. Zhu, J. Yue, M. Zhang, A. L. Antaris, J. Yuan, R. Cui, H. Wan, Y. Zhou, W. Wang, N. F. Huang, J. Luo, Z. Hu and H. Dai, *Nat. Commun.*, 2017, **8**, 737.

50 S. Wang, Y. Fan, D. Li, C. Sun, Z. Lei, L. Lu, T. Wang and F. Zhang, *Nat. Commun.*, 2019, **10**, 1058.

51 S. Zhu, S. Herraiz, J. Yue, M. Zhang, H. Wan, Q. Yang, Z. Ma, Y. Wang, J. He, A. L. Antaris, Y. Zhong, S. Diao, Y. Feng, Y. Zhou, K. Yu, G. Hong, Y. Liang, A. J. Hsueh and H. Dai, *Adv. Mater.*, 2018, **30**, e1705799.

52 H. Wan, J. Yue, S. Zhu, T. Uno, X. Zhang, Q. Yang, K. Yu, G. Hong, J. Wang, L. Li, Z. Ma, H. Gao, Y. Zhong, J. Su, A. L. Antaris, Y. Xia, J. Luo, Y. Liang and H. Dai, *Nat. Commun.*, 2018, **9**, 1171.

53 S. Zhu, Q. Yang, A. L. Antaris, J. Yue, Z. Ma, H. Wang, W. Huang, H. Wan, J. Wang, S. Diao, B. Zhang, X. Li, Y. Zhong, K. Yu, G. Hong, J. Luo, Y. Liang and H. Dai, *Proc. Natl. Acad. Sci. U. S. A.*, 2017, **114**, 962–967.

54 G. Hong, A. L. Antaris and H. Dai, *Nat. Biomed. Eng.*, 2017, **1**, 0010.

55 S. Daneshmand, A. K. Schuckman, B. H. Bochner, M. S. Cookson, T. M. Downs, L. G. Gomella, H. B. Grossman, A. M. Kamat, B. R. Konety, C. T. Lee, K. S. Pohar, R. S. Pruthi, M. J. Resnick, N. D. Smith, J. A. Witjes, M. P. Schoenberg and G. D. Steinberg, *Nat. Rev. Urol.*, 2014, **11**, 589–596.

56 A. K. Parchur, Z. Fang, J. M. Jagtap, G. Sharma, C. Hansen, S. Shafiee, W. Hu, Q. R. Miao and A. Joshi, *Biomater. Sci.*, 2020, DOI: 10.1039/d0bm00873g.

57 D. M. Montana, M. Nasilowski, W. R. Hess, M. Saif, J. A. Carr, L. Nienhaus and M. G. Bawendi, *ACS Appl. Mater. Interfaces*, 2020, **12**, 35845–35855.

58 Y. Feng, S. Zhu, A. L. Antaris, H. Chen, Y. Xiao, X. Lu, L. Jiang, S. Diao, K. Yu, Y. Wang, S. Herraiz, J. Yue, X. Hong, G. Hong, Z. Cheng, H. Dai and A. J. Hsueh, *Chem. Sci.*, 2017, **8**, 3703–3711.

59 R. Tian, H. Ma, Q. Yang, H. Wan, S. Zhu, S. Chandra, H. Sun, D. O. Kiesewetter, G. Niu, Y. Liang and X. Chen, *Chem. Sci.*, 2019, **10**, 326–332.

60 R. Tian, Q. Zeng, S. Zhu, J. Lau, S. Chandra, R. Ertsey, K. Hetti, T. Teraphongphom, Z. Hu, G. Niu, D. O. Kiesewetter, H. Sun, X. Zhang, A. L. Antaris, B. R. Brooks and X. Chen, *Sci. Adv.*, 2019, **5**, eaaw0627.